Enhanced molybdenum(VI) removal using sulfide-modified nanoscale zerovalent iron: kinetics and influencing factors

J. J. Lian, M. Yang, H. L. Wang, Y. Zhong, B. Chen, W. L. Huang and P. A. Peng

ABSTRACT

The overall goal of this study is to investigate the effect of sulfidated nanoscale zerovalent iron (S-nZVI) on the removal of hexavalent molybdate (MoO_4^{2-}) under different aquatic chemistry conditions. Surface analysis suggests that Mo(VI) is removed mainly by adsorption and co-precipitation onto the surface of S-nZVI and a small amount of Mo(VI) can be reduced to Mo(V) species. The results of batch tests show that Mo(VI) removal by S-nZVI are well described with the pseudo-second-order adsorption model. The removal rate increases with a decrease in solution pH (4.0–9.0) and is significantly affected by the S/Fe ratio of S-nZVI, with the optimal S/Fe ratio being 0.5. The presence of anions WO_4^{2-} or CrO_4^{2-} can reduce the Mo(VI) removal, which is likely because they compete for adsorption sites on the solid surfaces. The divalent cations Ni^{2+}, Cu^{2+} and Co^{2+} also inhibit the removal of Mo(VI) whereas Zn^{2+}, Ca^{2+} and Mg^{2+} enhance it. After being aged for 35 d in water, S-nZVI still exhibits high reactivity towards Mo(VI) removal (57.39%). The study demonstrates that S-nZVI can be used as an environmentally friendly material for effectively removing Mo(VI) from contaminated water.

Key words | adsorption, hexavalent molybdenum, nanoscale zero valent iron, reduction, sulfidation

HIGHLIGHTS

- S-nZVI was more reactive with Mo(VI) than was fresh nZVI.
- The S:Fe molar ratio had a significant effect on S-nZVI reactivity.
- The pseudo-second-order adsorption model was a good fit for the reaction process.
- S-nZVI maintained high Mo(VI) removal efficiency after 35 days' aging.
- Mo(VI) was removed through adsorption, co-precipitation, and reduction.

J. J. Lian
M. Yang
B. Chen
College of Energy and Environment,
Anhui University of Technology,
Ma'anshan, Anhui 243002,
China

H. L. Wang
Y. Zhong (corresponding author)
P. A. Peng
State Key Laboratory of Organic Geochemistry,
Guangdong Provincial Key Laboratory of Environmental Protection and Resources and Utilization, Guangdong-Hong Kong-Macao Joint Laboratory for Environmental Pollution and Control,
Guangzhou Institute of Geochemistry, Chinese Academy of Sciences,
Guangzhou 510640,
China
E-mail: *zhongyin@gig.ac.cn*

W. L. Huang
Department of Environmental Sciences, Rutgers,
The State University of New Jersey,
14 College Farm Road,
New Brunswick, NJ 08901,
USA

H. L. Wang
University of Chinese Academy of Sciences,
Beijing 100049,
China

doi: 10.2166/wst.2020.570

GRAPHICAL ABSTRACT

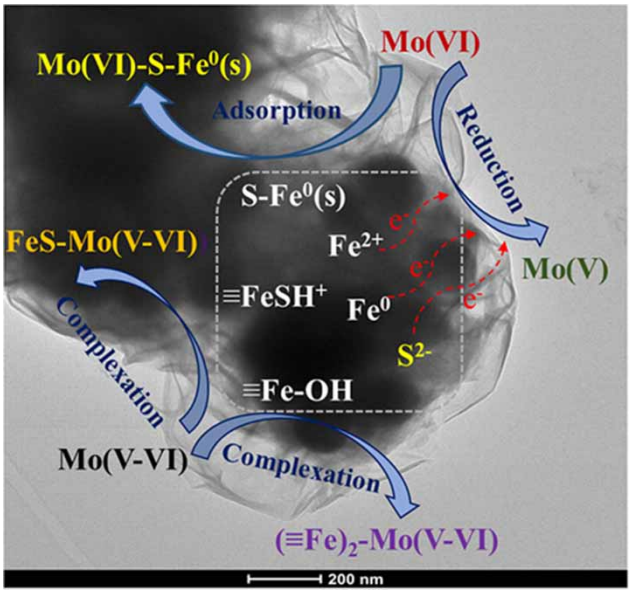

INTRODUCTION

Although molybdenum (Mo) at low levels is an essential micronutrient for both plants and animals, it has various adverse health effects on aquatic organisms when its concentration exceeds 5 mg/L in water (Moret & Rubio 2003). Subchronic and chronic oral exposures can result in sterility, growth retardation, hypothyroidism, anemia, liver or kidney abnormalities, and death (Namasivayam & Sangeetha 2006). Hexavalent molybdate (MoO_4^{2-}) is the most soluble species of Mo (Ma *et al.* 2015) and is the dominant species in molybdenum-contaminated industrial wastewaters in the manufacture of paints and ceramics, metal alloys, missiles and aircraft, solid lubricants, and pigments for printing inks (Namasivayam & Sureshkumar 2009). Indeed, Mo is widely detected in industrial wastewater, rivers, lakes, and groundwater, and Mo concentration in some waters has seriously exceeded 5 mg/L (Table S1). Therefore, effective technology is needed for removing Mo(VI) from contaminated waters.

Various technologies have been studied for Mo(VI) removal from waters, including chemical precipitation (Mamtaz & Bache 2001), ion-exchange (Polowczyl *et al.* 2017), and adsorption (Shan *et al.* 2016). Among these methods, adsorption has gained wide acceptance because of high efficiency, low cost and easy operation (Lou *et al.* 2015). However, most adsorption studies for Mo(VI) removal are carried out in an oxic environment, and there are few studies on Mo(VI) removal in anoxic water bodies. Iron monosulfide (FeS) is an important natural reductive mineral that exists extensively in soil, river sediment, underground water and coastal waters (Richard & Luther 2007). It plays important roles in the sorption, immobilization, and transformation of a variety of heavy metals and inorganic oxyanions in reducing environments, because of unique molecular structure and surface chemical properties (Morse & Arakaki 1993; Gong *et al.* 2016; An *et al.* 2017). Note that FeS has a very important influence on the geochemical cycle of molybdenum, because the content of soluble molybdenum in sulfide sediments, estuaries, and other reducing environments is extremely low (Crusius *et al.* 1996; Morgan *et al.* 2012). It is presumed that Mo(VI) may be reduced to MoS_2, or it may be associated with iron sulfide, or sulfide ferrous minerals have undergone synergistic precipitation (Bostick & Fendorf 2003). Nanoscale zerovalent iron (nZVI), as an environmental green material (Li *et al.* 2009), has a large surface area and is inexpensive, highly reducible, suitable for onsite operation, and can be magnetically separated (Cundy *et al.* 2008; Fan *et al.* 2009; Fu *et al.* 2014; Guan *et al.* 2015). The use of nZVI for

removing heavy metals ions, such as Mo(VI), Pb(II), Cr(VI), and As(V), from contaminated water and soil has shown promising results (Yan *et al.* 2010; Boparai *et al.* 2011; Huang *et al.* 2013). It has been reported that nZVI can remove Mo(VI) by adsorption of Mo(VI) onto the surface of nZVI followed by reduction to Mo(IV) (Qian *et al.* 2018). However, Fe^0 is easily passivated in water, rapidly lowering the rate of Mo(VI) reduction.

Recent studies show that sulfide-modified nZVI (S-nZVI) has higher reactivity, longevity and selectivity than nZVI and has great potential for the environmental remediation of heavy metals (Wu *et al.* 2018). It has been shown to increase precipitation and inhibit outer-sphere complexation for arsenic removal and to increase electron transfer from the nZVI core to the surface of Cr(VI) (Li *et al.* 2018; Wu *et al.* 2018). It can be expected that S-nZVI could be used for the removal of Mo(VI) from contaminated water. However, S-nZVI has not yet been studied for Mo(VI) removal; the specific mechanisms and the key influencing factors are not clear. Therefore, the goal of this study is to investigate S-nZVI for Mo(VI) removal from aqueous solution under anoxic conditions. Because S:Fe molar ratio plays an important role in the synthesis of S-nZVI, three S:Fe molar ratios (0.1, 0.5, and 1.0) on the structure of S-nZVI and the removal of Mo(VI) were examined. Also, we comprehensively analyzed, characterized and compared the composition, structure and morphology of S-nZVI before and after reaction with Mo(VI) to determine the mechanisms of Mo(VI) removal. To comprehensively evaluate Mo(VI) removal capacity by S-nZVI, the potential influences of pH, initial Mo(VI) concentration, S-nZVI dose, cation content, competing anions, ionic strength, and aging time were also studied. The obtained results would provide a theoretical reference for the treatment of Mo(VI) pollution in anoxic water bodies. It is crucial for the cognition of the migration and transformation process of Mo(VI) pollution in anoxic water bodies (such as groundwater and bottom water bodies of rivers and lakes).

MATERIAL AND METHODS

Materials

Chemicals used in this study were analytical grade (see Text S1 in Supporting Information for more details). Experiments were conducted in a gloved anaerobic chamber with an atmosphere of high purity nitrogen (99.99%).

Synthesis of nZVI and S-nZVI

Both nZVI and S-nZVI were synthesized using the method described by Li *et al.* (2016), with minor modification. In each trial, 180 mL of 0.3 M $NaBH_4$ solution containing a variable amount of $Na_2S_2O_4$ was added to 60 mL of 0.2 M $FeCl_2$ solution to obtain a black precipitate of S-nZVI (S:Fe molar ratios = 0.1, 0.5, and 1.0) or nZVI. The precipitate was centrifuged at 8,000 rpm for 5 min, washed in deoxygenated deionized water (three times) and then used in the experiments.

Batch experiments

All batch experiments were conducted anaerobically at constant temperature in the anaerobic chamber using 100 mL screw-capped vials as reactors, unless specified otherwise. The batch reactors were wrapped to keep them dark and mixed using a magnetic stirrer at 180 rpm. The samples were collected at regular time intervals in a 10 mL syringe and analyzed immediately after they were filtered through a 0.45 mm filter membrane. Batch experiments were conducted to examine the effects of four factors on the removal of Mo(VI) by S-nZVI: S:Fe ratio (0.1, 0.5 or 1.0); initial dose of S-nZVI (200, 500, 800 or 1,000 mg/L); and Mo(VI) concentration (20, 50, 80 or 100 mg/L). Such a concentration range of Mo(VI) has been found in various environments (Table S1). The enrichment of molybdenum in the iron sulfides environment is usually accompanied by the change of the solution pH (Bostick & Fendorf 2003). Therefore, the solution pH (4.0–9.0) was adjusted by buffer solutions (Bostick & Fendorf 2003) to obtain a constant ionic strength that allows for comparison between different experiments. The equilibrium pH was adjusted with different pH buffers: HAc–NaAc (pH 4–5), MOPS–NaAc (pH 6–7), H_3BO_3–$Na_2B_4O_7$ solution (pH 8–9). The experimental control conditions were constant: S:Fe ratio 0.5; pH 7.0; Mo(VI) concentration 50 mg/L; and S-nZVI dose 500 mg/L. When one of the four factors was investigated, the other three factors were kept at constant values. Note that control pH was 7.0 rather than 4.0 to examine the effect of initial Mo(VI) concentration and S-nZVI dose on Mo(VI) removal by S-nZVI because preliminary experiments showed that the reaction rate parameter of Mo(VI) at pH 4.0 was too rapid to be determined accurately. The results were analyzed using pseudo-first-order, pseudo-second-order, and Weber–Morris diffusion kinetics models to quantify Mo(VI) removal efficiency. Details of the models and the methodology of determining the parameters are provided in Supporting Information (Text S2).

Experiments were also conducted to investigate the influence of other factors on the removal of Mo(VI) by S-nZVI: co-existing cations (Zn^{2+}, Ca^{2+}, Mg^{2+}, Cu^{2+}, Ni^{2+} and Co^{2+}, used as their respective 0.01 M chlorates); and competing anions (WO_4^{2-}, in the form of a 0.5 mM sodium salt, basically consistent with Mo(VI) concentration, and CrO_4^{2-} as a 0.1 M sodium salt). The effect of ionic strength was tested in the presence of 0.05–0.5 mol/L KCl or without background electrolyte. These experiments were conducted under experimental conditions similar to those described above. Both 500 mg/L S-nZVI particles and 100 mL deoxygenated deionized water were introduced into the 100 mL screw-capped vials to investigate the effect of aging time on removal of Mo(VI) by S-nZVI. To simulate the environment of natural anoxic water bodies, the vials were sealed and placed in a dark room for aging. The aged samples were collected after various time intervals (0, 1, 7, 14, 21, 28 or 35 d) and used for Mo(VI) removal following the procedure described above.

Analytical methods

Separate experiments were conducted to investigate changes in surface morphology and structure of S-nZVI before and after reaction with Mo(VI). In each trial, after 1 h reaction with Mo(VI), the S-nZVI suspension was centrifuged at 8,000 rpm for 5 min. The S-nZVI solids were dried under nitrogen and used for surface analysis. Concentrations of Mo(VI) and total Fe ions were measured by flame analysis using a polarized Zeeman atomic absorption spectrophotometer (Hitachi ZA3000). All experiments were conducted in triplicate, and the results presented as mean value ± standard deviation. All graphs were drawn using Origin 8.5. Details of the analytical methods for surface characterization of the synthetic S-nZVI are given in Text S3 in Supporting Information.

RESULTS AND DISCUSSION

Mo(VI) removal by S-nZVI

S-nZVI with different S:Fe molar ratios (0, 0.1, 0.5 or 1.0) was obtained by adding different concentrations of $Na_2S_2O_4$ during nZVI synthesis. As shown in Figure 1(a), the performance of S-nZVI in removing Mo(VI) is strongly influenced by the S:Fe molar ratio. When the S:Fe molar ratio was initially increased from 0 to 0.5, Mo(VI) removal efficiency increased from 12.46% to 88.73%. That is, the Mo(VI) removal efficiency of S-nZVI with S:Fe ratio 0.5

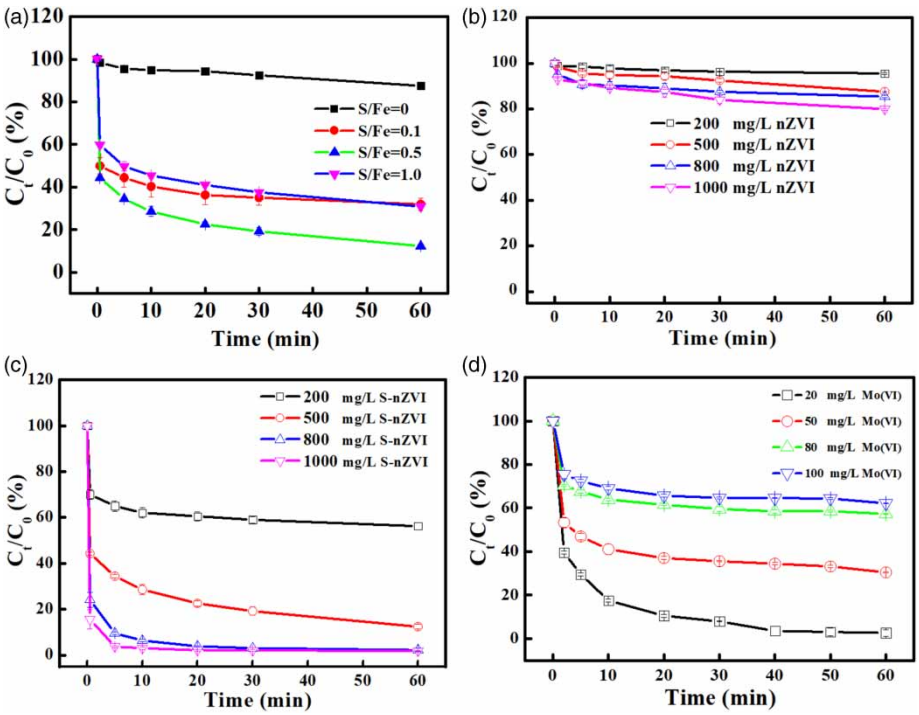

Figure 1 | Effect of (a) nZVI with different S/Fe molar ratios (50 mg/L Mo(VI), 500 mg/L S-nZVI), (b) initial nZVI dose (50 mg/L Mo(VI)), (c) initial S-nZVI dose (50 mg/L Mo(VI), S/Fe molar ratio = 0.5), and (d) initial Mo(VI) concentration (500 mg/L S-nZVI, S/Fe ratio = 0.5) on Mo(VI) removal at pH = 7.0 and T = 25 °C; error bars present mean ± standard deviation).

was seven times greater than that of nZVI. This increase in Mo(VI) removal by S-nZVI is explained as follows. Sulfur binds with Mo(VI) to increase the adsorption of Mo(VI) on the surface of S-nZVI; increased sulfur on the surface creates more binding sites for molybdenum (Helz *et al.* 2004). However, as the S:Fe molar ratio increased from 0.5 to 1.0, Mo(VI) removal efficiency decreased from 88.73% to 69.16%, indicating that higher sulfur content decreased Mo(VI) removal efficiency of S-nZVI. The quantity of released Fe in the final supernatant after Mo(VI) reaction with S-nZVI was determined for different S:Fe ratios. The results showed that dissolved Fe in the solution after Mo(VI) was reacted with S-nZVI was at a lower concentration than when Mo(VI) was reacted with nZVI (Figure S1), indicating that sulfidation inhibited corrosion of nZVI. Moreover, the FeS layer may be an electron conductor that accelerated the multi-electron transfer from the Fe^0 core to Mo(VI) oxyanions, as described by Du *et al.* (2016). Obviously, S-nZVI with an S:Fe ratio of 0.5 (S-$nZVI_{0.5}$) was clearly most effective in Mo(VI) removal. Other studies have also found that S-$nZVI_{0.5}$ has very high reactivity with tetrabromobisphenol A and hexabromocyclododecane (Li *et al.* 2016, 2017).

The effects of initial dose on Mo(VI) removal by nZVI and S-$nZVI_{0.5}$ at pH 7.0 are shown in Figure 1(b) and 1(c). The results show that, at the same dose, nZVI is much less effective than S-$nZVI_{0.5}$ in removing Mo(VI). Also, Mo(VI) removal efficiency increased rapidly from 43.79% to 98.20% within 60 min of the reaction beginning as S-nZVI dose increased from 200 to 1,000 mg/L (Figure 1(c)). The explanation for this is that the surface area and number of reaction sites both increased on S-nZVI particles, thus improving the removal of Mo(VI). When the initial concentration of MoO_4^{2-} increased from 20 to 100 mg/L, there was a significant decrease in Mo(VI) removal efficiency from 97.41% to 37.85% within 60 min of the reaction beginning (Figure 1(d)). The number of available S-nZVI adsorption sites did not change, but a greater initial concentration of MoO_4^{2-} requires more adsorption sites for complete removal; if there are insufficient sites available, the removal rate will decrease for a higher initial concentration.

S-nZVI surface analysis

To identify the surface reaction mechanisms of S-nZVI with Mo(VI), the surface of S-nZVI was investigated. Brunauer–Emmett–Teller specific surface area (BET-SSA) analysis showed that the specific surface areas of S-nZVI particles with S:Fe ratios of 0.1–1.0 were about 30–40 times larger than those of nZVI (Table S2). Moreover, the specific surface area of S-$nZVI_{0.5}$ was larger than that of S-$nZVI_{1.0}$, which helps to explain the Mo(VI) removal efficiency decrease as S:Fe molar ratio increased from 0.5 to 1.0. Transmission electron microscopy (TEM) showed that the structure of unmodified nZVI appeared to be chains of spherical particles with smooth surfaces, while S-$nZVI_{0.5}$ particles had a core of nZVI surrounded by a flake-like shell (Figure 2). After reaction with Mo(VI), the core–shell structure of S-$nZVI_{0.5}$ disappeared. A rough structure and flocculent precipitate formed on the surface, likely due to molybdenum binding and oxidation of divalent iron ions (Sun *et al.* 2017). Energy-dispersive X-ray spectroscopy (EDS) confirmed the presence of Fe, S, and Mo on the surface of S-nZVI after reacting with Mo(VI) (Figure S2). The elemental maps of Fe, S, and Mo suggested that these elements were well dispersed, which is consistent with EDS analysis.

X-ray photoelectron spectroscopy (XPS) showed the composition and chemical state of Fe, S and Mo on the surface of S-nZVI (Figure 3 and Table S3). Table S3 shows that no peak for Fe^0 was observed in S-nZVI particles with S/Fe = 0.5 and 1.0, suggesting that the coating of iron oxide or iron sulfide on the surface of Fe^0 gradually tightened with the increase of S/Fe ratios. Moreover, the relative abundance of Fe(II)–O and S^{2-} on the surface of S-$nZVI_{0.5}$ decreased significantly after reaction with Mo(VI), providing direct evidence that both Fe(II) and S(II) are involved in the removal of Mo(VI). Two intense peaks for $Mo3d_{5/2}$ on the S-nZVI were observed at 230.57 and 232.32 eV, which were respectively attributed to Mo(V) (Chen *et al.* 1998) and Mo(VI) (Delporte *et al.* 1995). This observation suggests that adsorbed Mo(VI) can be reduced to Mo(V) species by S-nZVI. The relative abundance of Mo(V) on the surface of S-$nZVI_{0.5}$ was greater than that of S-$nZVI_{0.1}$ or S-$nZVI_{1.0}$ (Table S3), which suggests that S-$nZVI_{0.5}$ had a higher reductive capacity for Mo(VI) removal. The relative abundances of Mo(V) and Mo(VI) shown in Table S3 suggest that most Mo(VI) was removed by adsorption through co-precipitation of Fe(III)/Mo hydroxide (Bostick & Fendorf 2003) rather than reduction, and the possible reaction mechanism of Mo(VI) by S-$nZVI_{0.5}$ at pH 7.0 is shown in Equations (1) and (2).

$$MoO_4^{2-} + Fe^0 + Fe^{2+} + S^{2-} \rightarrow Mo^{V}O_xS_y + Fe^{3+} + SO_3^{2-} + H_2O \quad (1)$$

$$\equiv Fe - OH + MoO_4^{2-} = \equiv Fe - O_2MoO_2^- + OH^- \quad (2)$$

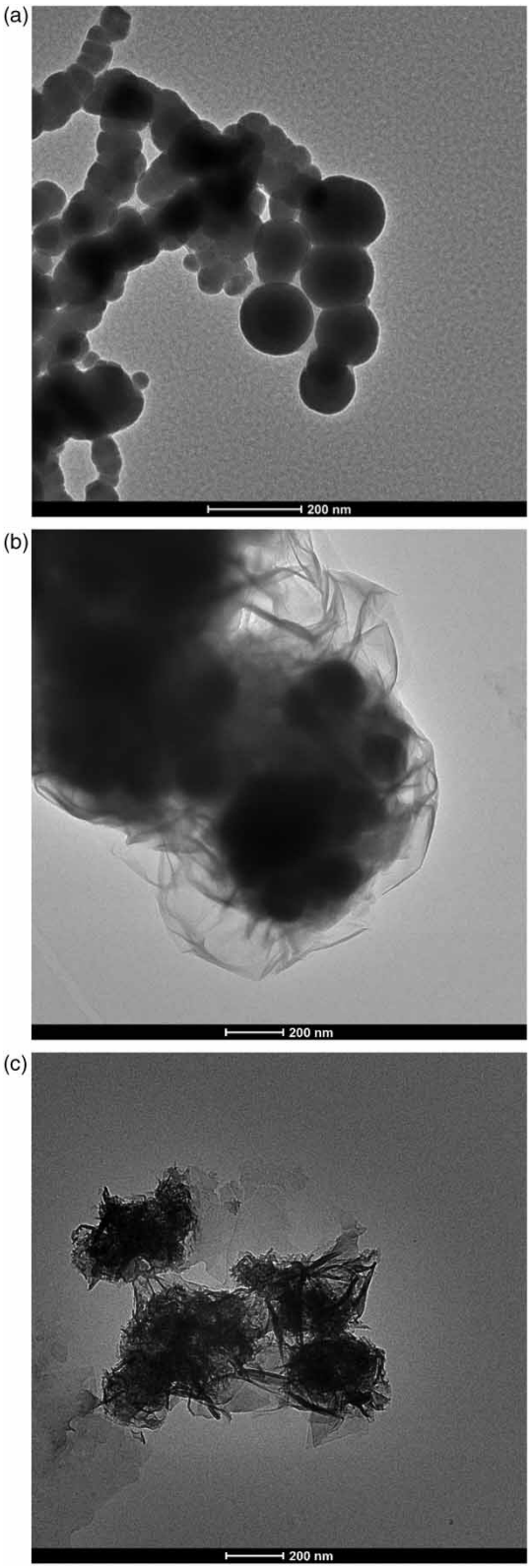

Figure 2 | TEM images of (a) unmodified nZVI, (b) S-nZVI$_{0.5}$ before the reaction with Mo(VI), and (c) S-nZVI$_{0.5}$ after the reaction with Mo(VI) (50 mg/L Mo(VI), 500 mg/L S-nZVI, S/Fe molar ratio = 0.5, pH = 7.0).

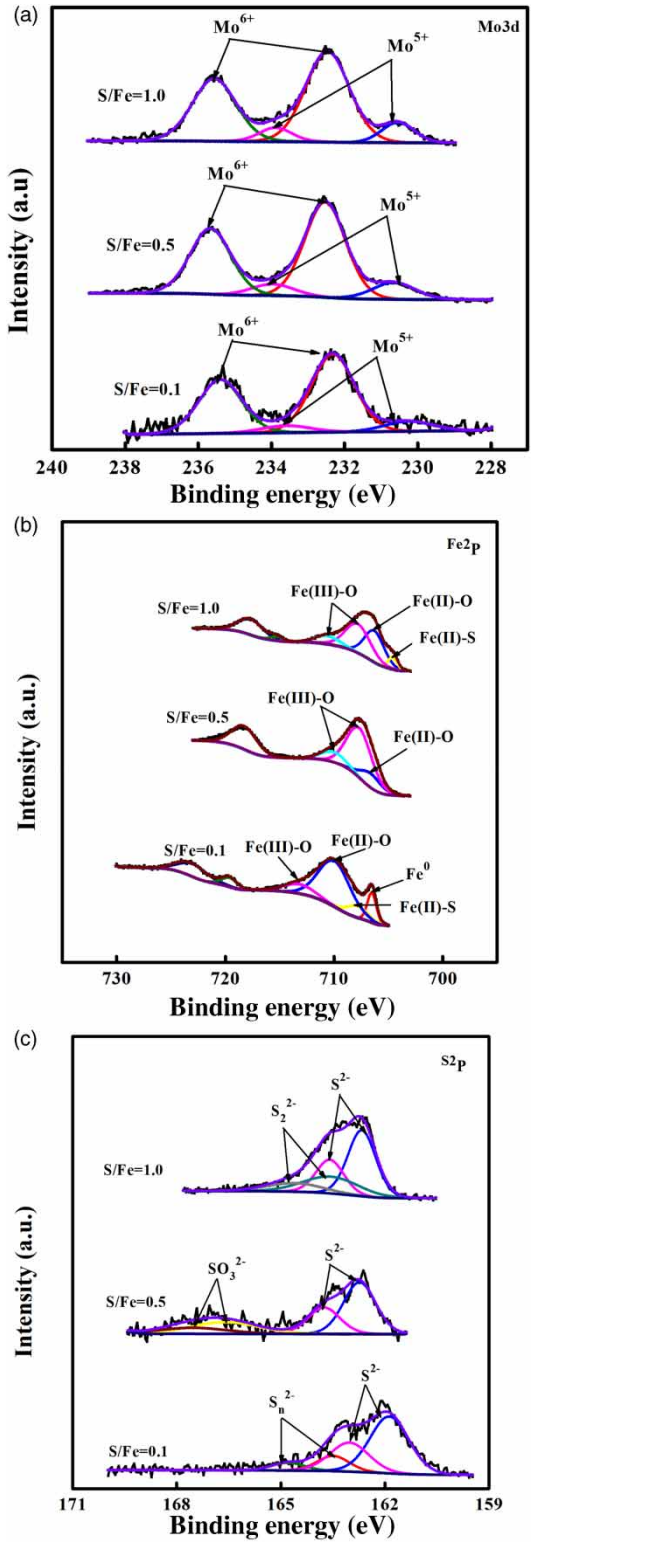

Figure 3 | XPS spectra of Mo(VI) treated with S-nZVI with different S/Fe ratios, and narrow scans of (a) Mo3d, (b) Fe2p, (c) S2p (50 mg/L Mo(VI), 500 mg/L S-nZVI 0.5 molar ratio of S/Fe, pH = 7.0, black and purple represent the original and the sum total of other colored lines, respectively). Please refer to the online version of this paper to see this figure in color: http://dx.doi.org/10.2166/wst.2020.570.

Table 1 | Comparison of pseudo-first-order and pseudo-second-order kinetics constants for Mo(VI) removal by S-nZVI particles (initial pH = 7.0, S/Fe molar ratio = 0.5, T = 25 °C)

		Initial concentration of Mo(VI) (mg/L)				Initial concentration of S-nZVI (mg/L)			
Parameter		**20**	**50**	**80**	**100**	**200**	**500**	**800**	**1,000**
Pseudo-first-order reaction kinetics	$k_1 \times 10^{-2}$ (1/min)	5.95	1.10	0.69	0.430	0.23	2.02	4.440	1.26
	R^2	0.970	0.828	0.908	0.90	0.881	0.952	0.898	0.775
Pseudo-first-order adsorption kinetics	$k_1 \times 10^{-2}$ (1/min)	7.46	4.83	6.51	6.03	1.60	1.90	3.72	2.61
	q_e (mg/g)	16.78	21.12	27.66	21.12	17.25	27.55	6.203	2.705
	R^2	0.971	0.957	0.980	0.974	0.742	0.954	0.905	0.798
Pseudo-second-order adsorption kinetics	$k_2 \times 10^{-2}$ (g/(mg·min))	1.86	1.04	1.07	0.87	4.43	1.88	2.88	4.80
	q_e (mg/g)	38.17	68.49	81.30	59.52	34.48	66.67	83.33	83.33
	R^2	0.999	0.998	0.999	0.999	0.997	0.991	1.000	1.000

Kinetics of Mo(VI) removal

The preceding solution and solid phase analyses suggest that there are three main stages of Mo(VI) removal: aqueous Mo(VI) oxyanions diffused to the water–S-nZVI interface, a process that is driven by valence forces and electrostatic attraction between sulfide ions, iron ions and Mo(VI) oxyanions; Mo(VI) was adsorbed at the solid–liquid interface by co-precipitation; and Mo(VI) was simultaneously reduced to Mo(V). Thus, the removal of Mo(VI) using Fe^0-based materials is a multi-step process that involves adsorption as well as a subsequent Mo(VI) reduction (Huang *et al.* 2012; Qian *et al.* 2018). To describe the Mo(VI) removal route by S-nZVI$_{0.5}$, pseudo-first-order and pseudo-second-order kinetics models were used to represent the reaction (Figure S3 and Table 1). It was observed that the experimental data fitted well with the pseudo-second-order adsorption model, with high correlation coefficients ($R^2 > 0.996$). The adsorption capacity obtained by the experiment (61.25 mg/g) was found to be close to the theoretical values (65.36 mg/g; reaction conditions: Mo(VI) concentration 50 mg/L, S-nZVI$_{0.5}$ concentration 500 mg/L, pH 7.0) predicted by the pseudo-second-order kinetic model. These data show that the pseudo-second-order adsorption model best represented the adsorption process, which implies that chemisorption was the rate-limiting process for Mo(VI) removal.

Solute adsorption onto the solid surface can be controlled by several steps, e.g., external diffusion, surface diffusion, and pore diffusion (Debnath & Ghosh 2009). In order to confirm the actual rate-controlling step in the Mo(VI) adsorption process, the well-known Weber–Morris equation was applied (Weber & Morris 1963). The plots of q_t versus $t^{0.5}$ are given in Figure S4 for the adsorption of Mo(VI) by S-nZVI$_{0.5}$ at different initial Mo(VI) concentrations and S-nZVI$_{0.5}$ dose. Obviously, the adsorption data were well-fitted by two straight lines, indicating that two steps took place during Mo(VI) adsorption onto S-nZVI$_{0.5}$. The detailed fitting model parameters are shown in Table 2. The R^2 values are close to unity, also confirming the applicability of the Weber–Morris model for Mo(VI) adsorption on S-nZVI$_{0.5}$. Firstly, Mo(VI) in aqueous solution was transported onto the surface of S-nZVI$_{0.5}$, then Mo(VI) was transported and adsorbed on the interior surface of S-nZVI$_{0.5}$ (Mittal *et al.* 2007). Also, the time in intraparticle diffusion state is longer than that of external diffusion state, indicating that the intraparticle diffusion is the main rate-controlling state.

Table 2 | Kinetic parameters of Weber–Morris model for Mo(VI) adsorption by S-nZVI particles (initial pH = 7.0, S/Fe molar ratio = 0.5, T = 25 °C)

		First stage			Second stage		
Variable	**C_0 (mg/L)**	**I_1**	**$k_{i,1}$ (g/(mg·min$^{0.5}$))**	**R^2**	**I_2**	**$k_{i,2}$ (g/(mg·min$^{0.5}$))**	**R^2**
S-nZVI	200	68.78	8.30	0.988	84.59	3.22	0.997
	500	50.95	6.48	0.991	61.29	3.47	0.982
	800	43.10	5.97	0.995	57.35	0.53	0.996
	1,000	39.26	3.92	0.985	48.28	0.12	0.994
Mo(VI)	20	17.03	5.04	0.999	31.36	1.03	0.986
	50	37.07	6.97	0.992	54.20	1.89	0.993
	80	38.74	5.99	0.995	55.35	1.59	0.985
	100	38.81	7.30	0.999	65.21	0.88	0.996

Effect of pH on Mo(VI) removal

The initial solution pH was changed from 4.0 to 9.0 to investigate the effect of pH on MoO_4^{2-} removal by S-nZVI. As shown in Figure 4(a), after 60 min, removal efficiency of Mo(VI) was 3.3%, 10.1%, 78.0%, 89.6%, 93.8% and 91.6% at pH of 9.0, 8.0, 7.0, 6.0, 5.0 and 4.0, respectively, suggesting that Mo(VI) removal increased with the decrease in solution pH. Preferential removal of Mo(VI) in an acidic solution is consistent with previous adsorption results (Lian *et al.* 2019). Acidity usually affects adsorption by changing the form of Mo(VI) and altering the surface zeta potential of adsorbents. The predominating ionic species of Mo(VI) were obtained from the Visual MINTEQ 3.0 software calculation. Obviously, MoO_4^{2-} at a concentration of 50 mg/L can be changed to other species that are more favorable for adsorption by electrostatic interaction at pH 4.0–7.0, such as $Mo_8O_{26}^{4-}$, $HMo_7O_{24}^{5-}$ or $Mo_7O_{24}^{6-}$ (Figure 4(c)). Zeta potential of S-nZVI was measured as a function of pH to determine the surface charge. The pH of point of zero change (pHpzc) of S-nZVI was calculated to be around 7.6 (Figure 4(b)). Thus, the positive surface charge attracted the negatively charged Mo(VI) species when pH was <7.6. When pH increased to be above pHpzc, electrostatic repulsion between the negatively charged surface of S-nZVI and negatively charged Mo(VI) species inhibited the adsorption of Mo(VI) and decreased removal efficiency. Nevertheless, the removal efficiency of Mo(VI) at pH = 4.0 was lower than that at pH = 5.0, which may be due to the change in the iron sulfides species. Richard & Luther (2007) reported that FeS can react with H^+ to form Fe^{2+} and HS^- under very acid condition. The loss of FeS on the surface of S-nZVI may contribute to the decrease in the capability of S-nZVI towards Mo(VI) removal.

Effects of ionic strength, competing anions and co-existing cations

Ionic strength affects binding of Mo(VI) with adsorbates by influencing the thickness and interface potential of the double electron layer of the adsorbents (Sari *et al.* 2007). Ionic strength can be used to distinguish between outer-sphere complexation and inner-sphere complexation. The influence of ionic strength on immobilization of Mo(VI) onto S-nZVI is shown in Figure 5(a). Increase in KCl concentration from 0 to 0.1 mol/L resulted in a decrease of 2.28 percentage points (from 67.58% to 65.30%) in the Mo(VI) removal rate. Outer-sphere complexation was inferred to be the removal mechanism of Mo(VI) because outer-sphere surface complexes are more susceptible to change in ionic strength than inner-sphere surface complexes (Kim *et al.* 2013). One reason for the decrease in Mo(VI) removal rate is the high concentration of Cl^-, which competed with MoO_4^{2-} for the positively charged adsorption sites on S-nZVI (Elwakeel *et al.* 2009).

The presence of anions (WO_4^{2-} and CrO_4^{2-}) also decreased the Mo(VI) removal rate (Figure 5(b)) because S-nZVI was positively charged during the reaction (as shown in Figure 4(b))

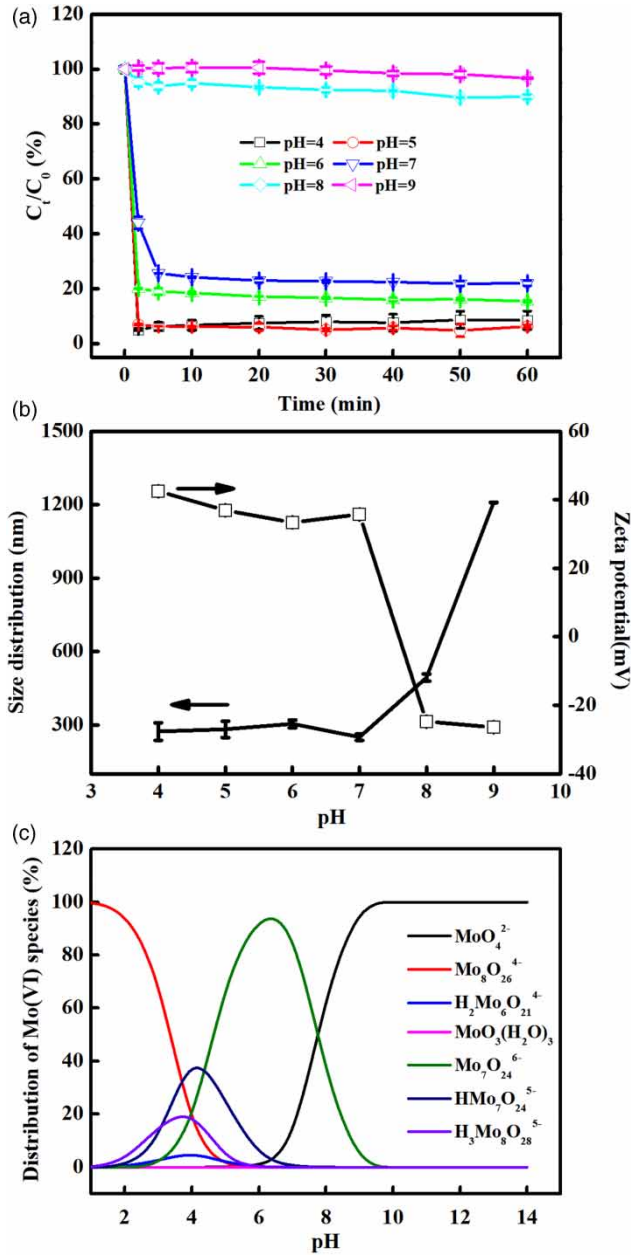

Figure 4 | Effect of pH on (a) Mo(VI) removal by S-nZVI (50 mg/L Mo(VI), 500 mg/L S-nZVI, S/Fe molar ratio = 0.5), (b) size distribution and zeta potential of S-nZVI with 0.5 molar ratio of S/Fe, and (c) distribution of Mo(VI) species (Mo(VI) concentration = 50 mg/L, T = 25 °C, ion strength = 0.1 M KNO_3); error bars present mean ± standard deviation.

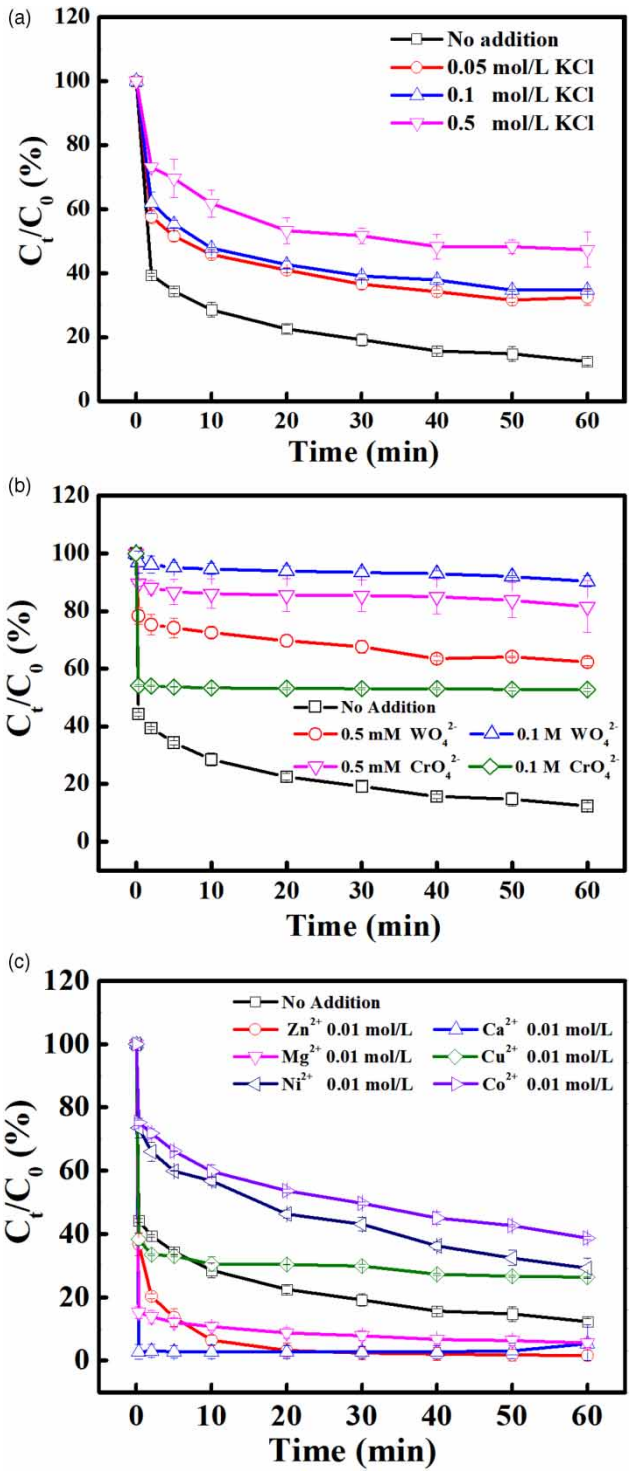

Figure 5 | Effect of (a) KCl concentration, (b) competing anions, (c) co-existing cations on Mo(VI) removal by S-nZVI (T = 25 °C, pH = 7.0, 50 mg/L Mo(VI), 500 mg/L S-nZVI with 0.5 molar ratio of S/Fe, error bars present mean ± standard deviation).

and electrostatically attracted the negative anions. Thus the two oxyacid ions competed for adsorption of MoO_4^{2-} on S-nZVI. However, a high concentration of CrO_4^{2-} reduced the inhibitory effect of the reaction, which was different from the effect of WO_4^{2-}. Ferrous ions are oxidized by Cr(VI) at the solid–solution interface, but not in aqueous solution, and the thickness of the iron oxide shells can be a barrier for electron transfer (Du *et al.* 2016). Divalent or trivalent iron on the adsorbent surface showed good adsorption and complexation of Mo(VI) (Lian *et al.* 2019; Lian *et al.* 2020). Figure 5(c) shows the effect of co-existing cations on the removal of Mo(VI) from aqueous solution onto S-nZVI. Co-existing cations present in natural water (such as Zn^{2+}, Ca^{2+} or Mg^{2+}) increase Mo(VI) removal. An explanation of this effect is that the standard reduction potentials of Mg^{2+}, Zn^{2+} and Ca^{2+} ($E_0 = -2.37$, -0.76 and -2.87 V, respectively) are less than that of Fe^{2+} ($E_0 = -0.45$ V), and thus any of the three free cations may form some covalent compound with Mo(VI), such as $CaMoO_4$. The specific chemical reaction needs further study. Cu^{2+}, Co^{2+} and Ni^{2+} that usually present in industrial wastewater have inhibitory effect on the Mo(VI) removal by S-nZVI. Cu^{2+}, Co^{2+} and Ni^{2+} ($E_0 = +0.34$, -0.28 and -0.26 V, respectively) have greater positive standard reduction potentials than Fe^{2+} and may occupy more active sites on the surface of S-nZVI. In other words, they may result in insufficient adsorption sites for Mo(VI) reactions.

Effect of aging

The removal efficiency of Mo(VI) of fresh nZVI and S-nZVI was 12.46% and 85.49%, respectively. After S-nZVI particles were aged in water for 35 days, the removal efficiency of Mo(VI) was 57.39%, which is still higher than that of fresh nZVI. It suggested that the aged S-nZVI had a higher capacity for Mo(VI) removal than freshly-prepared nZVI (Figure 6). It is consistent with the results of previous studies that S-nZVI has higher longevity than nZVI (Li *et al.* 2016). It is generally accepted that sulfidation of nZVI can inhibit the H_2 evolution reaction (reduction of water by Fe^0 to form hydrogen), reduce the Fe^0 corrosion (Chin *et al.* 2005; Liu & Lowry 2006), decrease the magnetic force of aged S-nZVI (Kim *et al.* 2014), and therefore improve the long-term performance of nZVI in the removal of contaminant. Overall, S-nZVI is more stable and long-lasting than nZVI in its capacity to remove Mo(VI).

CONCLUSIONS

This is the first report on the reactivity of S-nZVI towards Mo(VI) under various aquatic chemistry conditions. S-nZVI had higher reactivity towards Mo(VI) than did nZVI. Surface

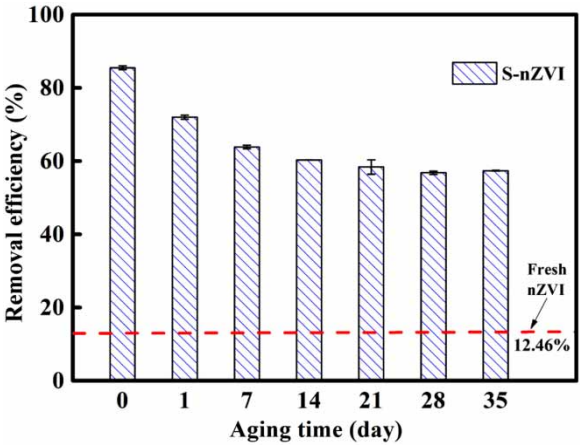

Figure 6 | Mo(VI) removal efficiency of aged S-nZVI (50 mg/L Mo(VI), 500 mg/L S-nZVI with 0.5 molar ratio of S/Fe, T = 25 °C, error bars present mean ± standard deviation).

analysis indicated that Mo(VI) could be removed by adsorption, co-precipitation, and reduction. The Mo(VI) removal by S-nZVI is well described with the pseudo-second-order adsorption model. Batch experiments showed that S-nZVI removed Mo(VI) at faster rate under acidic to neutral pH (4.0–7.0) than alkaline condition. The ions WO_4^{2-}, CrO_4^{2-}, Ni^{2+}, Cu^{2+} and Co^{2+} inhibited the removal of Mo(VI) whereas Zn^{2+}, Ca^{2+} and Mg^{2+} enhanced it. Aging experiments demonstrated that S-nZVI after aging of 35 days in water still had greater Mo(VI) removal capacity compared to nZVI, indicating the feasibility of S-nZVI for treatment of Mo(VI)-contaminated waters under anoxic condition.

ACKNOWLEDGEMENTS

This work was financially supported by the National Natural Science Foundation of China (Nos. 51709001, 41773132 and 42077285), Guangdong Foundation for Program of Science and Technology Research (Nos. 2017B030314057, 2020B1212060053 and 2019B121205006), the State Key Laboratory of Organic Geochemistry, GIGCAS (No. SKLOG2020-4), and the China Scholarship Council for Jianjun Lian (No. 201808340035).

DATA AVAILABILITY STATEMENT

All relevant data are included in the paper or its Supplementary Information.

REFERENCES

An, X. L., Huang, F. G., Rend, H. T., Wang, Y. F., Chen, Y., Liu, Z. M., Zhang, H. W. & Han, X. 2017 Oxidative dissolution of amorphous FeS and speciation of secondary Fe minerals: Effects of pH and As(III) concentration. *Chemical Geology* **462**, 44–54.

Boparai, H. K., Joseph, M. & O'Carroll, D. M. 2011 Kinetics and thermodynamics of cadmium ion removal by adsorption onto nano zerovalent iron particles. *Journal of Hazardous Materials* **186**, 458–465.

Bostick, B. C. & Fendorf, S. 2003 Differential adsorption of molybdate and tetrathiomolybdate on pyrite (FeS_2). *Environmental Science & Technology* **37**, 285–291.

Chen, G., Ford, T. E. & Clayton, C. R. 1998 Interaction of sulfate-reducing bacteria with molybdenum dissolved from sputter-deposited molybdenum thin films and pure molybdenum powder. *Journal of Colloid and Interface Science* **204**, 237–246.

Chin, P. P., Ding, J., Yi, J. B. & Liu, B. H. 2005 Synthesis of FeS_2 and FeS nanoparticles by high-energy mechanical milling and mechanochemical processing. *Journal of Alloys and Compounds* **390** (1–2), 255–260.

Crusius, J., Calvert, S., Pedersen, T. & Sage, D. 1996 Rhenium and molybdenum enrichments in sediments as indicators of oxic, suboxic and sulfidic conditions of deposition. *Earth and Planetary Science Letters* **145** (1–4), 65–78.

Cundy, A. B., Hopkinson, L. & Whitby, R. L. D. 2008 Use of iron-based technologies in contaminated land and groundwater remediation: a review. *Science of the Total Environment* **400**, 42–51.

Debnath, S. & Ghosh, U. C. 2009 Nanostructured hydrous titanium(IV) oxide: synthesis, characterization and Ni(II) adsorption behavior. *Chemical Engineering Journal* **152**, 480–491.

Delporte, P., Meunier, F., Pham-Huu, C., Vennegues, P., Ledoux, M. J. & Guille, J. 1995 Physical characterization of molybdenum oxycarbide catalyst: TEM, XRD and XPS. *Catalysis Today* **23**, 251–267.

Du, J. K., Bao, J. G., Lu, C. H. & David, W. 2016 Reductive sequestration of chromate by hierarchical FeS@Fe^0 particles. *Water Research* **102**, 73–81.

Elwakeel, K. Z., Atia, A. A. & Donia, A. M. 2009 Removal of Mo(VI) as oxoanions from aqueous solutions using chemically modified magnetic chitosan resins. *Hydrometallurgy* **97**, 21–28.

Fan, J., Guo, Y. H., Wang, J. J. & Fan, M. H. 2009 Rapid decolorization of azo dye methyl orange in aqueous solution by nanoscale zerovalent iron particles. *Journal of Hazardous Materials* **166**, 904–910.

Fu, F., Dionysiou, D. D. & Liu, H. 2014 The use of zero-valent iron for groundwater remediation and wastewater treatment: a review. *Journal of Hazardous Materials* **267**, 194–205.

Gong, Y. Y., Tang, J. C. & Zhao, D. Y. 2016 Application of Iron Sulfide Particles for Groundwater and Soil Remediation: A Review. *Water Research* **89**, 309–320.

Guan, X., Sun, Y., Qin, H., Li, J., Lo, I. M., He, D. & Dong, H. 2015 The limitations of applying zero-valent iron technology in

contaminants sequestration and the corresponding countermeasures: the development in zero-valent iron technology in the last two decades (1994–2014). *Water Research* **75**, 224–248.

Helz, G. R., Vorlicek, T. P. & Kahn, M. D. 2004 Molybdenum scavenging by iron monosulfide. *Environmental Science & Technology* **38**, 4263–4268.

Huang, Y. H., Tang, C. L. & Zeng, H. 2012 Removing molybdate from water using a hybridized zero-valent iron/magnetite/Fe(II) treatment system. *Chemical Engineering Journal* **200–202**, 257–263.

Huang, P. P., Ye, Z. F., Xie, W. M., Chen, Q., Li, J., Xu, Z. C. & Yao, M. S. 2013 Rapid magnetic removal of aqueous heavy metals and their relevant mechanisms using nanoscale zero valent iron (nZVI) particles. *Water Research* **47**, 4050–4058.

Kim, E. J., Murugesan, K., Kim, J. H., Tratnyek, P. G. & Chang, Y. S. 2013 Remediation of trichloroethylene by FeS-coated iron nanoparticles in simulated and real groundwater: effects of water chemistry. *Industrial & Engineering Chemistry Research* **52** (27), 9343–9350.

Kim, E. J., Kim, J. H., Chang, Y. S., Turcio-Ortega, D. & Tratnyek, P. G. 2014 Effects of metal ions on the reactivity and corrosion electrochemistry of Fe/FeS nanoparticles. *Environmental Science & Technology* **48** (7), 4002–4011.

Li, S., Yan, W. & Zhang, W. X. 2009 Solvent-free production of nanoscale zero-valentiron (nZVI) with precision milling. *Green Chemistry* **11**, 1618.

Li, D., Mao, Z., Zhong, Y., Huang, W. L., Wu, Y. D. & Peng, P. A. 2016 Reductive transformation of tetrabromobisphenol A by sulfidated nano zerovalent iron. *Water Research* **103**, 1–9.

Li, D., Zhu, X. F., Zhong, Y., Huang, W. L. & Peng, P. A. 2017 Abiotic transformation of hexabromocyclododecane by sulfidated nanoscale zerovalent iron: kinetics, mechanism and influencing factors. *Water Research* **121**, 140–149.

Li, J. X., Zhang, X. Y., Liu, M. C., Pan, B. C., Zhang, W. M., Shi, Z. & Guang, X. H. 2018 Enhanced reactivity and electron selectivity of sulfidated zerovalent iron toward chromate under aerobic conditions. *Environmental Science & Technology* **52**, 2988–2997.

Lian, J. J., Yang, M., Chen, B., Wang, S. S., Ye, T. R., Zheng, D. D. & Jiang, C. R. 2019 Characteristics and mechanisms of molybdenum(VI) adsorption by drinking water treatment residue. *Desalination and Water Treatment* **142**, 235–243.

Lian, J. J., Zhou, F. J., Chen, B., Yang, M., Wang, S. S., Liu, Z. L. & Niu, S. P. 2020 Enhanced adsorption of molybdenum(VI) onto drinking water treatment residues modified by thermal treatment and acid activation. *Journal of Cleaner Production* **244**, 118719.

Liu, Y. & Lowry, G. V. 2006 Effect of particle age (Fe^0 content) and solution pH on nZVI reactivity: H_2 evolution and TCE dechlorination. *Environmental Science & Technology* **40** (19), 6085–6090.

Lou, Z. N., Wang, J., Jin, X. D., Wan, L., Wang, Y., Chen, H., Shan, W. J. & Xiong, Y. 2015 Brown algae based new sorption material for fractional recovery of molybdenum and rhenium from wastewater. *Chemical Engineering Journal* **273**, 231–239.

Ma, W., Sha, X. L., Gao, L. L., Cheng, Z. H., Meng, F. Q., Cai, J., Tan, D. Z. & Wang, R. 2015 Effect of iron oxide nanocluster on enhanced removal of molybdate from surface water and pilot scale test. *Colloids and Surfaces A–Physicochemical and Engineering Aspects* **478**, 45–53.

Mamtaz, R. & Bache, D. H. 2001 Reduction of arsenic in groundwater by coprecipitation with iron. *Journal of Water Supply Research and Technology–Aqua* **50**, 313–324.

Mittal, A., Malviya, A., Kaur, D., Mittal, J. & Kurup, L. 2007 Studies on the adsorption kinetics and isotherms for the removal and recovery of Methyl Orange from wastewaters using waste materials. *Journal of Hazardous Materials* **148**, 229–240.

Moret, A. & Rubio, J. 2003 Sulphate and molybdate ions uptake by chitin-based shrimp shells. *Minerals Engineering* **16** (8), 715–722.

Morgan, B., Rate, A. W. & Burton, E. D. 2012 Trace element reactivity in FeS-rich estuarine sediments: influence of formation environment and acid sulfate soil drainage. *Science of the Total Environment* **438**, 463–476.

Morse, J. W. & Arakaki, T. 1993 Adsorption and coprecipitation of divalent metals with mackinawite (FeS). *Geochima et Cosmochimica Acta* **57**, 3635–3640.

Namasivayam, C. & Sangeetha, D. 2006 Removal of molybdate from water by adsorption onto $ZnCl_2$ activated coir pith carbon. *Bioresource Technology* **97** (10), 1194–1200.

Namasivayam, C. & Sureshkumar, M. V. 2009 Removal and recovery of molybdenum from aqueous solutions by adsorption onto surfactant-modified coir pith, a lignocellulosic polymer. *Clean–Soil Air Water* **37** (1), 60–66.

Polowczyl, I., Cyganowski, P., Urbano, B. F., Rivas, B. L., Bryjak, M. & Kabay, N. 2017 Amberlite IRA-400 and IRA-743 chelating resins for the sorption and recovery of molybdenum(VI) and vanadium(V): equilibrium and kinetic studies. *Hydrometallurgy* **169**, 496–507.

Qian, D. X., Su, Y. M., Huang, Y. X., Chu, H. Q., Zhou, X. F. & Zhang, Y. L. 2018 Simultaneous molybdate (Mo(VI)) recovery and hazardous ions immobilization via nanoscale zerovalent iron. *Journal of Hazardous Materials* **344**, 698–706.

Richard, D. & Luther, G. W. 2007 Chemistry of iron sulfides. *Chemical Reviews* **107** (2), 514–562.

Sari, A., Tuzen, M., Citak, D. & Soylak, M. 2007 Equilibrium, kinetic and thermodynamic studies of adsorption of Pb(II) from aqueous solution onto Turkish kaolinite clay. *Journal of Hazardous Materials* **149**, 283–291.

Shan, W. J., Shu, Y. N., Chen, H., Zhang, D. Y., Wang, W., Ru, H. Q. & Xiong, Y. 2016 The recovery of molybdenum(VI) from rhenium(VII) on amino-functionalized mesoporous materials. *Hydrometallurgy* **165**, 251–260.

Sun, Y., Lv, D., Zhou, J. S., Zhou, X. X., Lou, Z. M., Baig, S. A. & Xu, X. H. 2017 Adsorption of mercury (II) from aqueous solutions using FeS and pyrite: a comparative study. *Chemosphere* **185**, 452–461.

Weber, W. J. & Morris, J. C. 1963 Kinetics of adsorption on carbon from solution. *ASCE Sanitary Engineering Division Journal* **89**, 31–60.

Wu, D. L., Peng, S. H., Yan, K. L., Shao, B. B., Feng, Y. & Zhang, Y. L. 2018 Enhanced As(III) sequestration using sulfide-modified nano-scale zero-valent iron with a characteristic core–shell structure: sulfidation and As distribution. *ACS Sustainable Chemistry & Engineering* **6**, 3039–3048.

Yan, W., Herzing, A. A., Kiely, C. J. & Zhang, W. X. 2010 Nanoscale zerovalent iron (nZVI): aspects of the core-shell structure and reactions with inorganic species in water. *Journal of Contaminant Hydrology* **118**, 96–104.

First received 27 September 2020; accepted in revised form 16 November 2020. Available online 30 November 2020